Journal of Luminescence 134 (2013) 35–41

Contents lists available at SciVerse ScienceDirect

Journal of Luminescence

journal homepage: www.elsevier.com/locate/jlumin

Less contribution of nonradiative recombination in ZnO nails compared with rods

Yunfei Sun [a,b], Jinghai Yang [c,*], Lili Yang [c], Ming Gao [a,b,c], Xiaonan Shan [a], Zhiqiang Zhang [c], Maobin Wei [c], Yang Liu [c], Lianhua Fei [c], Hang Song [a]

[a] Key Laboratory of Excited State Processes, Changchun Institute of Optics, Fine Mechanics and Physics, Chinese Academy of Sciences, Changchun, 130033, People's Republic of China
[b] Graduate School of the Chinese Academy of Sciences, Beijing, 100049, People's Republic of China
[c] Institute of Condensed State Physics, Jilin Normal University, Siping, 136000, People's Republic of China

ARTICLE INFO

Article history:
Received 16 April 2012
Received in revised form
6 September 2012
Accepted 13 September 2012
Available online 23 September 2012

Keywords:
Nails
Nonradiative recombination
Photoluminescence

ABSTRACT

Well aligned ZnO nails with small heads and rods arrays have been grown on indium tin oxides (ITO) substrates by a simple hydrothermal method without any metal catalyst or additives. The optical properties of the as-grown ZnO microstructures were investigated by room-temperature and temperature-dependent photoluminescence spectra. From the PL spectra measured in the range of 80–300 K, the origins of near-band-gap UV lines have been identified in terms of bound exciton complexes and the phonon replicas. We also estimated that the activation energy of the temperature quenching for ZnO nails is higher than that of rods, indicating less nonradiative recombination contributes to the emission process in ZnO nails, which was further testified by the time-resolved PL results. Thus, the relative emission intensity ratio between UV and deep level emission in room-temperature PL spectra for nails is 2.3-times higher than that of rods.

1. Introduction

As one of II–VI semiconductor materials, low-dimensional ZnO nanostructures have great potential applications in photoelectronic devices due to their direct wide band gap (3.37 eV) and large exciton binding energy (60 meV). So far, ZnO nanowires [1–4], nanorods [5], nanobelts [6], nanotubes [7], ZnO nanonails [8–10], and various ZnO nanostructures have been prepared by various techniques. Among these ZnO nanostructures, ZnO nanonails have attracted uncountable attention due to their well defined geometry. However, nearly all the ZnO nanonails were fabricated by physical vapor deposition [11], thermal evaporation [8,12], chemical vapor deposition [13], and carbothermal method [14,15], which usually needs stiff conditions, such as high temperature [13,16], adding some catalysts or additives [15], vacuum or complicatedly controlled atmosphere [17–19]. In this paper, ZnO microstructures were synthesized via a simple hydrothermal synthesis route without any catalysts, which shows many advantages, such as low cost, low temperature, environment friendly and simple operation process. Especially, we have presented the detailed structural and optical properties of nail-like structure composed of a rod and a small head.

Moreover, as well as we known, the temperature-dependent PL is a very sensitive tool for characterizing the radiative and nonradiative recombination process in the materials, which is very helpful in understanding the optical performance and luminescence mechanism of the materials. However, the reports about the photoluminescence (PL) properties of ZnO nail-like structures mainly focused on the room-temperature PL spectra [20–22]. The research on the temperature-dependent photoluminescence spectra of ZnO nail-like structures is quite limited so far. Therefore, it is very necessary to systematically investigate the temperature-dependent PL properties of ZnO nails and rods for prompting their applications in luminescence device and solar cells.

2. Experiments

In our experiment, all chemicals (analytical grade reagents) were directly used without further purification. The ZnO nails and rods were synthesized on indium tin oxides (ITO) substrates with a hydrothermal reaction route. Before growth, the substrates were ultrasonically cleaned for 15 min in acetone, ethanol and deionized water in sequence. All the initial chemical solutions were prepared with deionized water. The detailed experiment process was described as follows: for the aqueous solutions to grow nails, zinc nitrate hexahydrate [$Zn(NO_3)_2 \cdot 6H_2O$, 99.0% purity] and hexamethyltetramine ($C_6H_{12}N_4$, 99.0% purity) were individually dissolved in 35 ml deionized water with a concentration of 0.1 M and 0.15 M

* Corresponding author. Tel.: +86 434 3290009; fax: +86 434 3294566.
E-mail address: jhyang1@jlnu.edu.cn (J. Yang).

0022-2313/$ - see front matter © 2012 Elsevier B.V. All rights reserved.
http://dx.doi.org/10.1016/j.jlumin.2012.09.021

respectively, which were mixed together and stirred for 10 min. Then the mixed solution was transferred into a Teflon-lined stainless steel autoclave with a capacity of 80 ml. The pretreated ITO substrates were immersed into the aqueous solution and tilted against the wall of the autoclaves with an angle of 60°. Finally, we sealed the Teflon-lined stainless steel autoclave and heat it at 95 °C for 11 h in an ordinary laboratory oven. Subsequently, the autoclave was cooled down to room-temperature. After thoroughly washing the substrates with deionized water and drying under air atmosphere, a white layer of product was formed on the ITO substrates. For ZnO rods, zinc nitrate hexahydrate [$Zn(NO_3)_2 \cdot 6H_2O$, 99.0% purity] and hexamethyltetramine ($C_6H_{12}N_4$, 99.0% purity) with a concentration of 0.1 M and 0.1 M were used, and all the other experimental conditions are identical as that of nails.

X-ray diffraction (XRD) patterns were recorded by a MAC Science MXP-18 X-ray diffractometer using a Cu target radiation source. Scanning electron microscopy (SEM) pictures were collected on a Hitachi, S-570 SEM. Transmission electron micrographs (TEM) and high-resolution transmission electron microscopy (HRTEM) images were taken on JEM-2100 transmission electron microscope. The room-temperature and temperature-dependent photoluminescence (PL) measurements were carried out on the Renishaw inVia micro-PL spectrometer. A continuous 325 nm light of a He–Cd laser was used as the excitation source. In the measurements of the temperature-dependent PL, the specimen was put into a liquid nitrogen cycling system, in which the temperature varied in the range of 80–300 K. Time-resolved PL (TRPL) was performed by using an excitation laser line from a frequency tripled sapphire:Ti laser emitting at 266 nm, a 0.3 m monochromator and a streak camera. The spectral resolution is about 1 meV and the time resolution is 7 ps. The measurements were done under weak excitation conditions (0.5 W/cm^2).

3. Results and discussions

Fig. 1(a and b) shows the XRD patterns of highly oriented ZnO nails and rods grown on ITO substrates by a hydrothermal method. All the observed diffraction peaks can be indexed to a wurtzite hexagonal-phase of pure ZnO (JCPDS card, No. 80-0074), which indicates no other impurity phase exists in the samples [23–25]. We can also notice that the intensity of the (0 0 2) diffraction peak located at 34.65° is the strongest in comparison with the other diffraction peak, which illustrates the highly preferential orientation of ZnO nails and rods arrays along *c*-axis [26]. In addition, we can also observe that the FWHM (full width at half maximum) of the nail is narrower than that of the rod, which indicates better crystallinity of the as-grown nails [27]. The EDAX spectra given in the inset of Fig. 1 show the presence of Zn, Si, In, Ca and O as the elementary components. Si, In, Ca can be attributed to ITO substrate, indicating that our samples are only composed of Zn and O elements.

To investigate the presence of different groups of ZnO nail and rod, the sample was characterized by Fourier transform infrared (FTIR) spectrophotometer. The FTIR spectra of the as-grown ZnO was shown in Fig. 2, which includes the following main characteristic absorption peaks: 3437, 1575, 1410, 1136, 993, 830, 619, and 539 cm^{-1}. The peaks at 3437 and 1410 cm^{-1} is the characteristic absorption of hydroxyl groups –OH which were come from water (solvent of the reactant). The peak at 1575 cm^{-1} can be attributed to the asymmetric $>C=O$ stretching frequency of the adsorbed HMT on the surface of ZnO. The picture exhibits the peak at 1136 cm^{-1}, indicating the existence of C–O group. The peaks at 993, 830 cm^{-1} correspond to C=C also from the reactant of HMT. The peaks at 619 and 539 cm^{-1} are corresponding to unsaturated bond and Zn–O respectively. We can see that the chemical groups attached on the surface of them are almost same. That is because that although the concentration of the initial solution are different, the chemical bond are identical between nails and rods due to the same chemical composition of the initial solutions. These results prove that organic groups are adsorbed to the surface of ZnO nails, which indicate that ZnO can be applied to organic and inorganic solar cells for its easily combination with organics.

Fig. 3 shows the SEM images of the as-grown ZnO nails and rods. From the tilted view, we can see that the large-scale, vertically aligned ZnO nails and rods were uniformly grown with high density over the entire surface of the ITO substrate. As shown in the high-magnification SEM images of Fig. 3(a and c), the diameters of nails and rods are no longer uniform along their whole length, but gradually decrease from the bottom to the top. Interestingly, in Fig. 3(a and b), each ZnO nail consists of a cap attached to a cone-shaped stem. Although the caps of the ZnO nails do not perform perfect hexagonal shape, they are basically

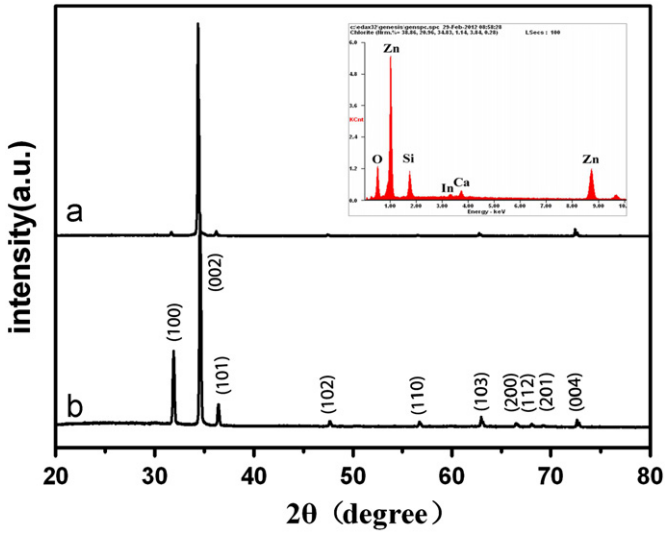

Fig. 1. Typical XRD patterns of ZnO nails (a) and ZnO rods (b),and the inset shows the EDAX spectrum of a representative ZnO nail sample.

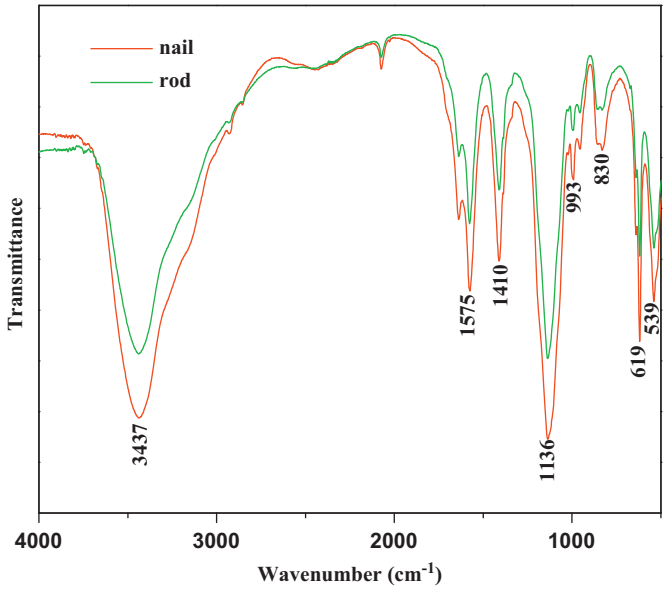

Fig. 2. FTIR spectra of as synthesized ZnO nail and rod.

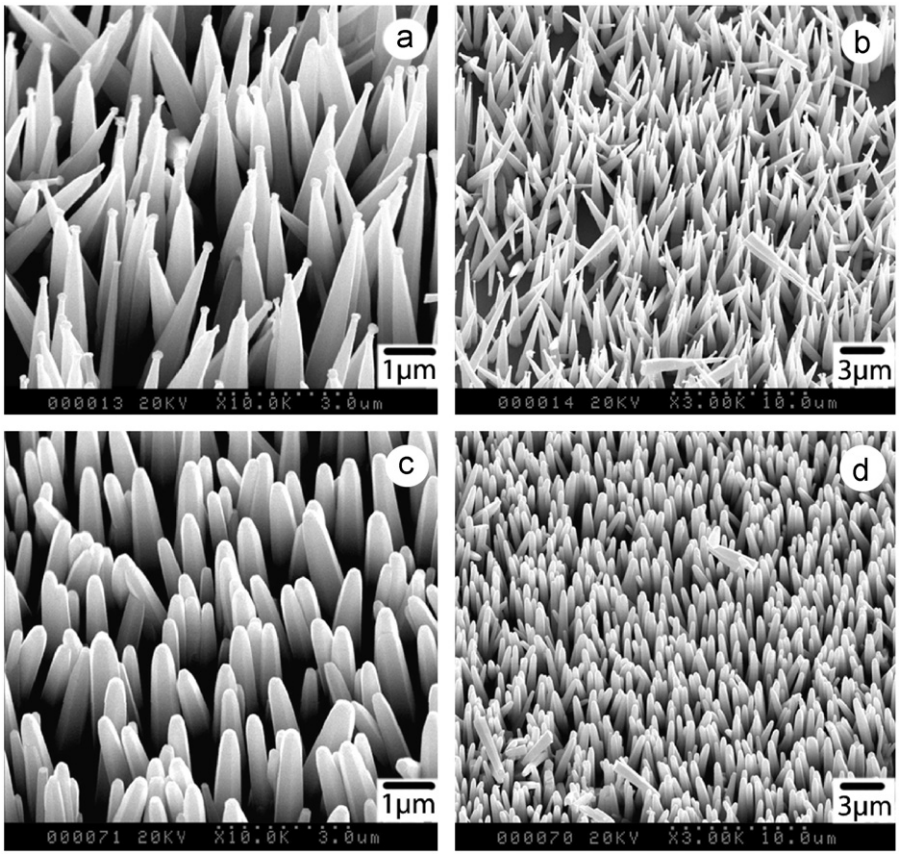

Fig. 3. Tilt-view SEM images of vertically aligned ZnO nails (a and b) and rods (c and d) synthesized at 95 °C by the hydrothermal method.

comprised of hexagonal facets [15]. The diameters of the cone-shaped stems range from ~600 nm at the bottom to ~200 nm at the top; the diameter of the hexagonal cap is ~300 nm. We can also see that the diameter of the nails stem decreased faster from the bottom to the top than that of rods.

ZnO crystal growth process consists of nucleation and growth, which is affected by the intrinsic crystal structure and the external conditions. In aqueous solution, Zn^{2+} is solvated by water, giving rise to aquo ions. In dilute solution, Zn^{2+} can exist as several monomeric hydroxyl species such as $Zn(OH)_2$ solid. As shown in our ZnO nail growth schematic diagram of Fig. 4, $Zn(OH)_2$ were adsorbed on ITO substrate when substrates were immersed into the aqueous solution with ITO faced down. Then solid ZnO nuclei are formed by the dehydration of these hydroxyl species. The ZnO crystal can continue to grow by the condensation of the surface hydroxyl groups with the zinc–hydroxyl complexes [29].

The controllable synthesis of ZnO nails and rods was achieved by varying the concentration of the reactant. It is reasonable to believe that the growth rates (R) perpendicular to (0 0 2) and {0 $\bar{1}$ 0} planes are changed with variable concentration of the reactant. If R(0 0 2) is larger than R{0 $\bar{1}$ 0} and each of them is invariable during the growth process of ZnO nanocrystals, the ZnO rods should be formed. If R{0 $\bar{1}$ 0} is larger than R(0 0 2), and each of them is unchanged, ZnO disks should be obtained. The formation of ZnO nails may arise from the change of R(0 0 2) and R{0 $\bar{1}$ 0} during the growth process of ZnO nanocrystals. According to our experimental results and our analysis, a possible kinetic mechanism to form ZnO nails was proposed. As illustrated in Fig. 4, when the hydrothermal system was heated to 95 °C, ZnO crystalline nuclei were formed by the hydrolysis–condensation reaction of Zn^{2+} ions. The zinc–hydroxyl complexes and $Zn(NO_3)_2$ in the solution diffused onto the surface of ZnO crystalline nuclei,

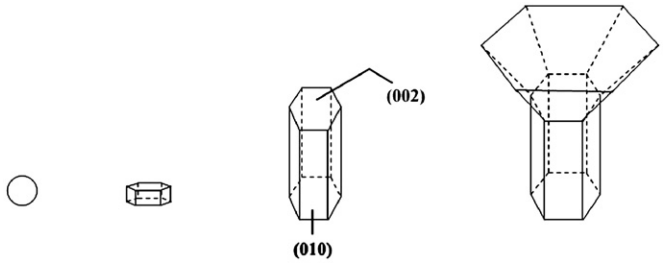

Fig. 4. Schematic diagram of nucleation and growth process of vertically aligned ZnO nails.

and reacted with the surface hydroxyl groups to maintain the growth of ZnO crystalline nuclei. The ZnO crystalline nuclei firstly grew into rod-like structures because R(0 0 2) is larger than R{0 $\bar{1}$ 0}.

Chemical reactions in the growth process of ZnO structures can be probably described as follows [28]:

$$C_6H_{12}N_4 + 6H_2O \leftrightarrow 6CH_2O + 4NH_3 \quad (1)$$

$$NH_3 + H_2O \rightarrow NH_4^+ + OH^- \quad (2)$$

$$Zn(NO3)_2 \rightarrow Zn^{2+} + 2NO_3 - \quad (3)$$

$$Zn^{2+} + 4NH_3 \rightarrow Zn(NH3)_4^{2+} \quad (4)$$

$$Zn^{2+} + 4OH^- \rightarrow Zn(OH)_4^{2-} \quad (5)$$

$$Zn(NH3)_4^{2+} + 2OH^- \rightarrow ZnO + 4NH_3 + H_2O \quad (6)$$

$$Zn(OH)_4^{2-} \rightarrow ZnO + H_2O + 2OH^- \quad (7)$$

From above reaction we can see that the over dose of $C_6H_{12}N_4$ not only produces excessive OH^-, but excessive NH_3 gas as shown

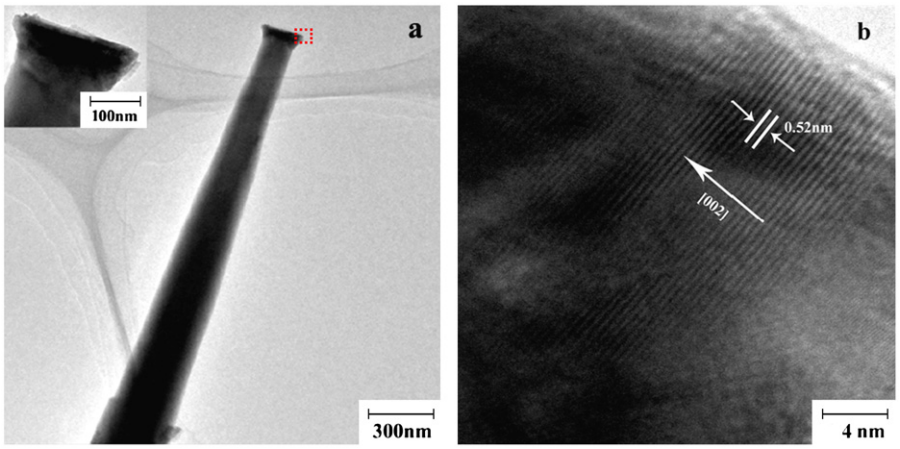

Fig. 5. (a) TEM image and (b) HRTEM image of the ZnO nails.

in the chemical reaction formulas (1, 4, and 6). Since the solution is sealed in the Teflon-lined stainless steel autoclave, the pressure in the autoclave will be strongly influenced by the NH_3 gas quantity. At the end of the reaction, the pressure in the autoclave will be very large with the increase of the NH_3. We infer that $R(0\ \bar{1}\ 0)$ will be promoted due to the large pressure in the reaction system. So $R(0\ 0\ 2)/R\{0\ \bar{1}\ 0\}$ will turn small and rod structure was evolved into a nail caused by the formation of a small head.

Further structural properties of the vertically aligned ZnO nails were checked by TEM, as shown in Fig. 5(a). It can be seen that these structures are several microns in length and the diameters of the stems decreased from the bottom to the top, which are in good accordance with the results observed under SEM. Fig. 5(b) of high resolution TEM (HRTEM) image reveals a lattice fringe of 0.52 nm, corresponding to the (0 0 2) fringes perpendicular to the growth direction. It further confirms that the ZnO nail is a wurtzite type structure with (0 0 2) preferential orientation.

The optical properties of as-grown ZnO structures were characterized by the PL spectroscopy at room-temperature. The PL spectra (Fig. 6(a)) of ZnO rods and ZnO nails consist of both dominant UV emission at 3.21 eV and weak deep level emission (DLE). The UV emission band is ascribed to a near band edge transition of ZnO, which originated from the recombination of the free excitons through an exciton–exciton collision process [30]. Its exact energy position depends on the contribution between the FX, FX-phonon replica and the transition between free electrons to acceptor bound holes [31]. While, with respect to the appearance of deep level emission in room-temperature PL spectra, there are many controversial standpoint and hypotheses to explain the defect emission [32–34]. The deep level emission (DLE) had been identified by many defect origins, such as V_O, V_{Zn}, O_i, Zn_i and so on [35–37]. In general, the relative intensity ratio between UV and DLE emission band (I_{UV}/I_{DLE}) can be used to characterize the optical properties of materials. The larger ratio the sample has, the fewer deep level defects exist in the sample. By calculation for Fig. 6(a), we found that the I_{UV}/I_{DLE} value for nails was 2.3-times higher than that of rods, which indicates that the as-grown ZnO nails should possess a better optical property in contrast with ZnO rods. Moreover, we can also conclude that the ZnO nails have less deep level defects, which has a good agreement with the XRD results above.

Room-temperature TRPL spectra in the UV region have been illustrated in Fig. 6(b). It is obvious that the lifetime of nails is about 2-times longer than that of rods, which is inconsistent with observed enhancement of total UV emission intensity in Fig. 6(a). The UV emission intensity is contributed by both radiative and nonradiative recombination. The lifetime difference indicates that the contribution of nonradiative process is different between nails and rods, i.e. more nonradiative contribution in rods than nails. The nonradiative recombination are mainly originated from the defects in the sample. ZnO grown in the chemical solution has two kinds of defects, i.e. surface defects and intrinsic defects. TRPL is a powerful method to monitor the existence of the surface recombination. As earlier demonstrated for ZnO nanorods [5,38], the surface recombination can strongly influence the decay time. The excess minority carriers via the near-band-gap recombination exhibit a single exponential decay or a non-exponential decay, depending on whether the surface recombination is the major recombination channel or not. Fig. 6(b) shows that both samples exhibit a single exponential decay in the TRPL spectra, which means no surface recombination contribute to the UV emission process. Then the nonradiative process is mainly caused by the intrinsic defects in the samples, indicating nails owns less intrinsic defects, which has a good agreement with the XRD and PL results.

We can see from Fig. 6(a) that the DLE band is very broad and asymmetric. According to the experimental data, a good fitting could be obtained when deconvolutions of two Gaussians are used for the spectra, which indicates that two kinds of deep-level-defect emission centers exist in the samples. As shown in Fig. 6(c), the green emission peak ($P1$) centered around 2.34 eV has been recently attributed to at least two different defect origins, i.e., V_O and V_{Zn} [39]. The yellow emission peak ($P2$) centered at 2.07 eV is usually ascribed to the oxygen interstitials O_i or Li impurities [40,41]. However, For Li element, which is the most common impurities we did not detect its signal from both the XRD and EDAX patterns, maybe its concentration is too lower to be detected. So we can infer that O_i and Li are possibly ascribed to be the reasons for the yellow emission. From the deep level emission fitted by Gaussian functions, we can see that the relative emission intensity ratio of I_{P1}/I_{P2} in PL spectrum of nails (0.8) is smaller than that of rods (1.2), which indicates that much more O_i and Li impurities exist in rods.

To further testified that less nonradiative recombination contribute to the UV emission process of ZnO nails, we studied the temperature-dependent PL spectra of the structures. With respect to the origins of these peaks, we firstly analyze the PL spectrum of the near band emission at 80 K as shown in Fig. 7. The domain peak at 3.338 eV can be attributed to doner bound exciton (D^0X) recombination [42,43]. Usually, the FX band in typical ZnO nanostructures under relative lower temperature cannot be clearly observed due to the existence of more bound excitons [44]. Without doubt, the same phenomenon happens in our case.

The weak feature observed at 3.354 eV can be assigned to the free exciton (FX) recombination [42]. In addition to the D^0X and FX peak, another three lines located at 3.314, 3.232 and 3.163 eV, respectively, also can be observed, which are probably related to the FX and their phonon replica [45]. Through detailed calculation and comparison, the peak at 3.314 eV can be assigned to the first-order transverse optical (TO) phonon replica of free exciton recombination (FX–TO) since the energy spacing between them is close to a TO energy [46]. The strong emission intensity of TO phonon peaks suggests a strong coupling of TO phonon and FX. The peak at 3.232 eV can be attributed to the FX emission accompanied by a TO and the first-order longitudinal optical (LO) phonons (FX–TO–LO) [23], since the energy difference between this line and the FX is close to the sum of the energies of a TO and a LO phonons. Similarly, the peaks at 3.163 eV is correspondingly assigned to the FX–TO–2LO emissions. This analysis is based closely on that made by Zhang et al. [45] for the study of sol–gel grown nanocyrstalline ZnO. However, the analysis raises some questions. As the FX–1TO feature is among the most intense parts of the PL spectra in Fig. 7, it would indicate that coupling to TO phonons is very strong, and so a corresponding feature would be expected at the FX–2TO position which is ~3.274 eV. Instead, the spectra in Fig. 7 have a clear minimum at this position so the identification of the 3.314 eV feature with FX–1TO recombination is questionable. Although we retain the FX–TO designation for the 3.314 eV feature in the discussion below, this remains open to correction.

As shown in the temperature-dependent PL spectra in Fig. 8, the well resolved emission lines of the free-exciton phonon replicas are thermally broadened and evolve into an asymmetric featureless PL curve [47, 48]. At the same time the intensity of the bound-exciton emissions rapidly decreases. From the results of the Fig. 8, it is clearly seen that the maximum of the PL spectrum coincides with the emission of 1TO phonon replica of the free excitons (FX–TO) becomes the strongest PL feature at temperatures higher than 200 K.

Fig. 8 also indicates the quite different intensity quenching behavior of ZnO nail and ZnO rod. Grabowska et al. reported that the quenching behavior of band edge emission is very important in evaluating the effect of nonradiative centers in ZnO nanostructure materials [49,50]. Normally, two competitive carrier quenching processes exist in the materials, one is radiative and the other is nonradiative. Nonradiative recombination rates are generally thermally activated [51]. If only one nonradiative recombination channel exists, the PL intensity dependent on the temperature can be described as below [49,50]

$$I = I_0/[1 + a\exp(-Ea/kT)] \quad (8)$$

where I is the PL intensity, a is the process rate parameter, k is the Boltzmann constant, and Ea is the activation energy.

The integrated PL intensity of ZnO nails and ZnO rods as a function of reciprocal temperature has been summarized in Fig. 9. We fitted all the experimental results with the Eq. (8) to extract the activation energy. In Fig. 9, we display the fitting curves and the corresponding fitting formulas. We can see that the activation energy of the temperature quenching is evaluated to be 56 meV for ZnO nails. And the corresponding activation energy of ZnO rods is evaluated to be 47 meV. Lin et al. points out that the lower activation energy is mainly due to the existence of more

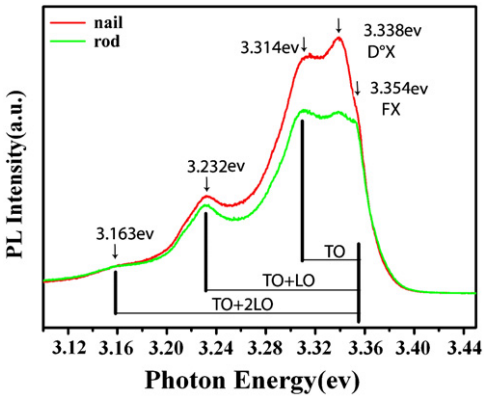

Fig. 7. Low-temperature (80 K) PL spectra of ZnO nails and rods.

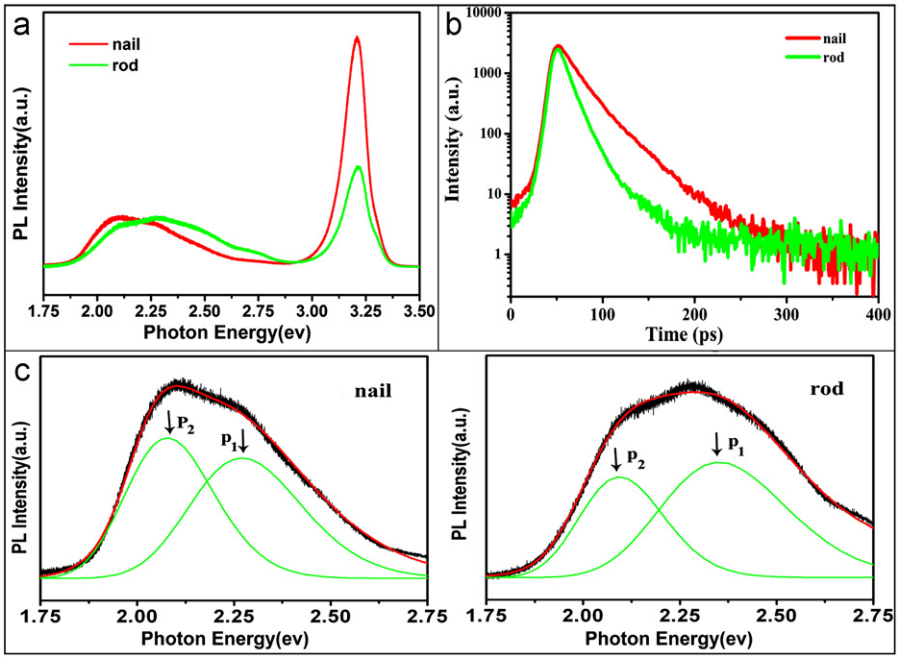

Fig. 6. (a) Room-temperature PL spectra of ZnO nails (red line) and ZnO rods (green line). (b) Time-resolved PL spectra of nails and rods in the UV region. (c) Deep level emission spectra of ZnO nails and rods. A good fitting could be obtained when deconvolutions of two Gaussian peaks ($P1$ and $P2$) are used for the spectra. (For interpretation of the references to color in this figure legend, the reader is referred to the web version of this article.)

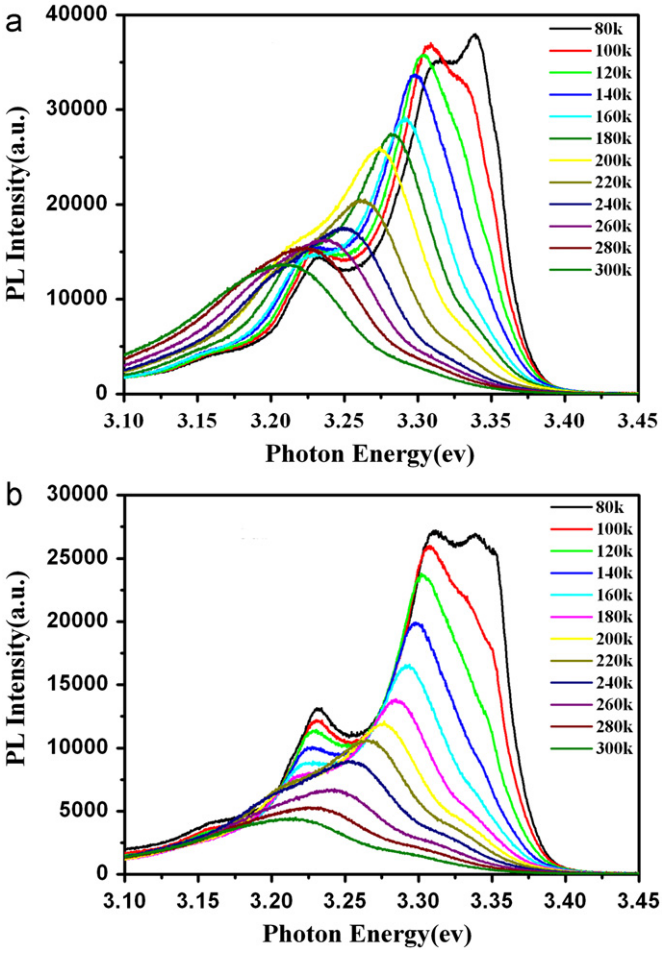

Fig. 8. Temperature-dependent PL spectra of (a) ZnO nails and (b) ZnO rods.

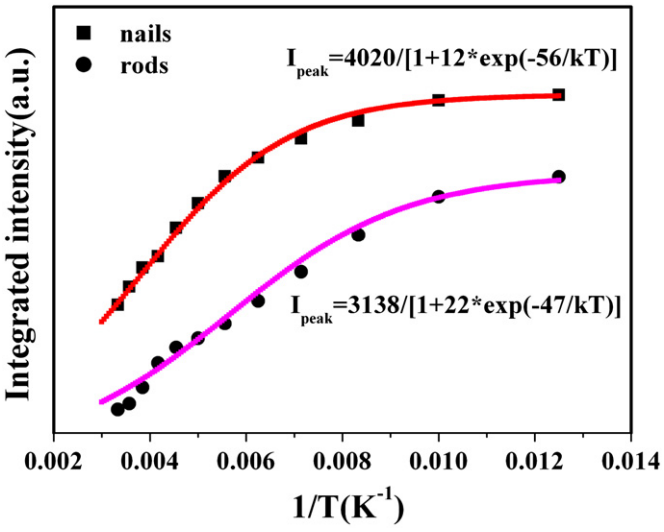

Fig. 9. Reciprocal temperature-dependent entire intensities of the ZnO nails and ZnO rods. The formulas and the solid lines in the figure are the results of simulation.

nonradiative contributions in the materials, which can be also deduced from the Eq. (8) [49]. Therefore, we can conclude that less nonradiative recombination contributes to the UV emission process in ZnO nails than that in ZnO rods, which have a great agreement with the temperature-dependent PL results and also well explains why the PL intensity of ZnO nails is higher than that of ZnO rods.

4. Conclusions

In this work, we have successfully synthesized ZnO nails and ZnO rods by a simple hydrothermal method. Both time-resolved PL and temperature-dependent PL spectra reveal a less nonradiative contribution in ZnO nails, which induces that the relative emission intensity ratio between UV and deep level emission in room-temperature PL spectra for nails is 2.3-times higher than that of rods. Our results will stimulate more investigation on ZnO nails and finally pave a way for ZnO nails in the application of laser, gas sensors, and solar energy conversion devices.

Acknowledgments

The authors acknowledge financial support from National Natural Science Foundation of China (Grant nos. 11204104, 61178074 and 61008051), Program for the Development of Science and Technology of Jilin province (Item nos. 20110415, 201115219 and 20100113), the Eleventh Five-Year Program for Science and Technology of Education Department of Jilin Province (Item nos. 20090422, 20110169 and 20110170), the Open Project Program for National Laboratory of Superhard Materials (No. 201004), Program for the Master Students' Scientific and Innovative Research of Jilin Normal University (Item nos. 201112, 201101, 201139).

References

[1] M.H. Huang, Y. Wu, H. Feick, N. Tran, E. Weber, P. Yang, Adv. Mater. 13 (2001) 113.
[2] R. Yousefi, M.R. Muhamad, A.K. Zak, Thin Solid Films 518 (2010) 5971.
[3] R. Yousefi, F.J. Sheini, M.R. Muhamad, M.A. More, Solid State Sci. 12 (2010) 1088.
[4] R. Yousefi, B. Kamaluddin, M. Ghoranneviss, F. Hajakbari, Appl. Surf. Sci. 255 (2009) 6985.
[5] Q.X. Zhao, L.L. Yang, M. Willander, B.E. Sernelius, P.O. Holtz, J. Appl. Phys. 104 (2008) 073526.
[6] Z.W. Pan, Z.R. Dai, Z.L. Wang, Science 291 (2001) 1947.
[7] J.H. Yang, J.H. Zheng, H.J. Zhai, L.L. Yang, Y.J. Zhang, J.H. Lang, M. Gao, J. Alloys Compd. 475 (2009) 741.
[8] G. Shen, Y. Bando, D. Chen, B. Liu, C. Zhi, D. Golberg, J. Phys. Chem. B 110 (2006) 3973.
[9] A. Umar, Y.B. Hahn, Cryst. Growth Des. 8 (2008) 2741.
[10] D.H. Fan, R. Zhang, X.H. Wang, Physica E 42 (2010) 2081.
[11] W. Ouyang, J. Zhu, Mater. Lett. 62 (2008) 2557.
[12] M.X. Qiu, Z.Z. Ye, J.G. Lu, H.P. He, J.Y. Huang, L.P. Zhu, B.H. Zhao, Appl. Surf. Sci. 255 (2009) 3972.
[13] S.W. Kim, S. Fujita, H.K. Park, B. Yang, H.K. Kim, D.H. Yoon, J. Cryst. Growth 292 (2006) 306.
[14] J. Liu, S. Lee, K.H. Park, Y.H. Ahn, J.Y. Park, K.H. Koh, J. Nanosci. Nanotechnol. 10 (2010) 6150.
[15] J.Y. Lao, J.Y. Huang, D.Z. Wang, Z.F. Ren, Nano Lett. 2 (2003) 235.
[16] S.N. Das, J.P. Kar, J.H. Choi, S. Byeon, Y.D. Jho, J.M. Myoung, Appl. Phys. Lett. 95 (2009) 111909.
[17] G.Z. Shen, J.H. Cho, C.J. Lee, Chem. Phys. Lett. 401 (2005) 414.
[18] X. Han, G. Wang, J. Jie, W.C.H. Choy, Y. Luo, T.I. Yuk, et al., J. Phys. Chem. B 109 (2005) 2733.
[19] B.H. Kong, D.C. Kim, H.K. Cho, Physica B 726 (2006) 376.
[20] G. Shen, Y. Bando, B. Liu, D. Golberg, C.-J. Lee, Adv. Funct. Mater. 16 (2006) 410.
[21] S. Kar, B.N. Pal, S. Chaudhuri, D. Chakravorty, J. Phys. Chem. B 110 (2006) 4605.
[22] X. Song, Y. Zhang, J. Zheng, X. Li, J. Phys. Chem. Solids 68 (2007) 1681.
[23] J.H. Yang, J.H. Zheng, H.J. Zhai, X.M. Yang, L.L. Yang, Y. Liu, J.H. Lang, M. Gao, J. Alloys Compd. 489 (2010) 51.
[24] R. Yousefi, A.K. Zak, M.R. Mahmoudian, J. Solid State Chem. 184 (2011) 2678.
[25] A.K. Zak, M.E. Abrishami, W.H.Abd. Majid, R. Yousefi, S.M. Hosseini, Ceram. Int. 37 (2011) 393.
[26] Z. Gu, M.P. Paranthaman, J. Xu, Z.W. Pan, ACS Nano 3 (2009) 273.
[27] C. Li, G.J. Fang, J. Li, L. Ai, B.Z. Dong, X.Z. Zhao, J. Phys. Chem. C 112 (2008) 990.
[28] L.L. Yang, Q.X. Zhao, M. Willander, J. Alloys Compd. 469 (2009) 623.

[29] L.N. Zhang, H.Q. Yang, J.H. Ma, L. Li, X.W. Wang, L.H. Zhang, S. Tian, X.Y. Wang, Appl. Phys. A 100 (2010) 1061.
[30] Y.C. Kong, D.P. Yu, B. Zhang, W.S. Fang, Q. Feng, Appl. Phys. Lett. 78 (2001) 407.
[31] G.Z. Xing, D.D. Wang, J.B. Yi, L.L. Yang, M. Gao, M. He, J.H. Yang, J. Ding, T.C. Sum, T. Wu, Appl. Phys. Lett. 96 (2010) 112511.
[32] B.D. Yao, Y.F. Chen, N. Wang, Appl. Phys. Lett. 81 (2002) 757.
[33] K. Vanheusden, C.H. Seager, W.L. Warren, D.R. Tallant, J.A. Voigt, J. Appl. Phys. 79 (1996) 7983.
[34] S.A. Studenikin, M. Cocivera, W. Kellner, H. Pascher, J. Lumin. 91 (2002) 223.
[35] Q.X. Zhao, P. Klason, M. Willander, Appl. Phys. Lett. 87 (2005) 211912.
[36] T.M. Borseth, B.G. Svensson, A.Y. Kuznetsov, P. Klason, Q.X. Zhao, M. Willander, Appl. Phys. Lett. 89 (2006) 262112.
[37] P. Klason, T.M. Børseth, Q.X. Zhao, Solid State Commun. 145 (2008) 321.
[38] L.L. Yang, Q.X. Zhao, M. Willander, X.J. Liu, M. Fahlman, J.H. Yang, Cryst. Growth Des. 10 (2010) 1904.
[39] J.H. Yang, R. Wang, L.L. Yang, J.H. Lang, M.B. Wei, M. Gao, X.Y. Liu, J. Cao, X. Li, N.N. Yang, J. Alloys Compd. 509 (2011) 3606.
[40] Y.W. Heo, D.P. Norton, S.J. Pearton, J. Appl. Phys. 98 (2005) 073502.
[41] D. Li, Y.H. Leung, A.B. Djurisic, Z.T. Liu, M.H. Xie, S.L. Shi, S.J. Xu, W.K. Chan, Appl. Phys. Lett. 85 (2004) 1601.
[42] Y.H. Shin, M.D. Kim, J. Korean Phys. Soc. 53 (2008) 2504.
[43] V.A. Fonoberov, K.A. Alim, A.A. Balandin, Phys. Rev. B 73 (2006) 165317.
[44] J.S. Jie, G.Z. Wang, Y.M. Chen, X.H. Han, Q.T. Wang, B. Xu, Appl. Phys. Lett. 86 (2005) 031909.
[45] Y. Zhang, B.X. Lin, X.K. Sun, Z.X. Fu, Appl. Phys. Lett. 86 (2005) 131910.
[46] F. Decremps, J.P. Porres, A.M. Saita, J.C. Cheervin, A. Polian, Phys. Rev. B 65 (2002) 092101.
[47] K. Ogata, T. Kawanishi, K. Maejima, K. Sakurai, S. Fujita, Jpn. J. Appl. Phys. 40 (2001) L657.
[48] S.-W. Kim, S. Fujita, Appl. Phys. Lett. 86 (2005) 153199.
[49] J. Grabowska, A. Meaney, K.K. Nanda, J.P. Mosnier, M.O. Henry, J.R. Duclere, E. McGlynn, Phys. Rev. B 71 (2005) 115439.
[50] S.S. Lin, H.P. He, Z.Z. Ye, B.H. Zhao, J.Y. Huang, J. Appl. Phys. 104 (2008) 114307.
[51] L.L. Yang, Q.X. Zhao, M.Q. Israr, J.R. Sadaf, M. Willander, G. Pozina, J.H. Yang., J. Appl. Phys. 108 (2010) 103513.